Optimal Designs of Wound Field Switched Flux Machines with Different DC Windings Configurations

Wenting Wang, *Student Member*, *IEEE*, Yuankui Wang, Enlin Ma, and Lijian Wu, *Senior Member, IEEE,*

***Abstract*—Wound field switched flux (WFSF) machines exhibits characteristics of the simple robust rotor, flexible flux-adjustable capability, and no risk of demagnetization. However, they suffer from a poor torque density compared with permanent magnet machines due to the saturation. Therefore, in this paper, two WFSF machines with single- and double-layer DC windings, respectively, are optimized for the maximum torque. The end-winding (EW) lengths differ in these two machines, which can affect the optimal design. Design parameters including the DC to armature winding copper loss ratio, slot area ratio and split ratio are optimized when two machines have the same copper loss and overall sizes. In addition, the influence of the flux density ratio, total copper loss, air-gap length and aspect ratio on the optimal split ratio is investigated using the finite element method and results are explained through the analytical model accounting for the saturation. It is discovered that the EWs have no effect on the optimal copper loss ratio, which is unity. In terms of the slot area ratio, the machine with single-layer DC windings prefers smaller DC slot areas than armature slot areas. In the WFSF machine with longer EWs, the optimal split ratio becomes smaller. Moreover, compared with other parameters, the flux density ratio can significantly affect the optimal split ratio.**

***Index Terms*—Design, End-winding, Optimization, Split ratio, Wound field switched flux machine.**

I. INTRODUCTION

PERMANENT magnet (PM) synchronous machines have gained much attention in recent years due to their merits of high efficiency and torque density, which are suited for many industrial applications. The stator-PM machines [1] including switched flux (SF) PM machines [2]-[5], flux reversal machines [6]-[7], and doubly salient PM machines [8], are one of the popular PM machine types. With magnets housed in the stator, these machines possess characteristics of easy heat dissipation and a simple robust rotor structure compared to rotor-PM machines [9]-[10]. Among them, SF PM machines stand out because of high torque density and outstanding anti-demagnetization capability and thus is favorable for electric vehicles and renewable energy applications. The use of PMs does, however, bring challenges including flexible flux adjustment and irreversible demagnetization. Moreover, expensive cost and limited supply of rare earths arouse new problems, especially in applications where the cost is sensitive. Therefore, these concerns are driving the surge of research interests in would field (WF) machines and hybrid excited (HE) machines [11]-[15].

The WFSF machines are developed getting merits of SF PM machines and WF machines. A typical 3-phase WFSF machine is developed from the 12/10 stator-/rotor- pole FSPM machine, as Fig. 1 shows [13]. In contrast to the conventional SFPM machine, the stator of the WFSF machine is integrated, similar to that of a switched reluctance machine. By replacing PMs with field windings, the space containing PMs becomes a slot with windings injected with DC currents. There are two types of WFSF machines with different DC coil connections: one has double-layer DC windings (Machine A) and the other has single layer DC windings (Machine B). These two machines are identical when the end-windings (EWs) are not taken into account. However, the EWs can affect the performance and optimal designs.

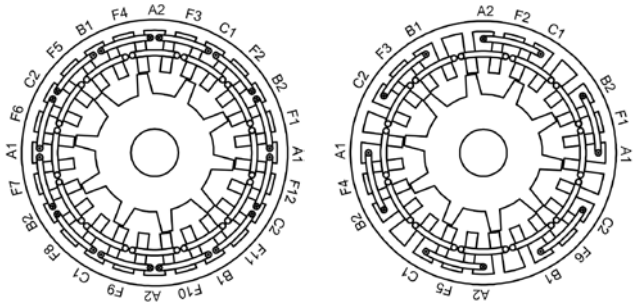

(a) (b)

Fig. 1. 12/10 stator-/rotor- pole WFSF machines with single and double-layer DC windings. (a) Double-layer (Machine A). (b) Single layer (Machine B).

Despite of the drawback associated with PMs, the WFSF machine has another weakness, i. e. the low torque density due to severe saturation. Consequently, design and optimization of WFSF machines are important research topics. The torque density has been improved by introducing various novel topologies. The WFSF machine with a segmental rotor was developed in [16] and studied in [17]. Due to shorter magnetic

Manuscript received October 25, 2022; accepted December 09, 2022. date of publication December 25, 2022; date of current version December 18, 2022.

This work was supported in part by the National Key R&D Program of China under 2019YFB1503700 and by the National Natural Science Foundation of China under Grant 51677169.

W. T. Wang and L. J. Wu are with Zhejiang University, Hangzhou, 3100005 China. (e-mail: wtwang_vera@zju.edu.cn;ljw@zju.edu.cn). Yuankui Wang and Enlin Ma are with China State Shipbuilding Corporation, Ltd..

(Corresponding Author: Lijian Wu)

Digital Object Identifier 10.30941/CESTEMS.2022.00047

flux paths in the rotor, this machine can generate a higher torque. The partitioned stator WFSF machine was also proposed, which allocates the DC and armature windings in two stators to fully utilize the inner space [18]. It can boost the average torque by 19% when compared to the conventional WFSF machine. Regarding the winding configuration, the influence of armature winding configurations on the average torque and torque ripple was analyzed in [19]. The half-teeth-wound armature windings can aid in achieving a larger torque because of the concentrated fluxes. Stator-/rotor-pole number combinations also play an important role. In [20], several 24-stator-slot WFSF machines with different rotor pole numbers were investigated and compared in terms of the back EMF, torque ripple and torque capability. The optimal rotor pole numbers, which are 13 and 14 for the 12-stator-slot WFSF machine, were discovered in [21] based on a lumped parameter magnetic circuit model. Moreover, the rotor pole arc being 0.3 is ideal for producing the largest torque, but the optimal stator designs are not involved [22].

In addition to adopting novel topologies and selecting proper the pole numbers, the optimization of design parameters is an additional effective way to achieve high torque density. WFSF machines differ from SF PM machines in specific design parameters, such as the DC to armature winding copper loss ratio and slot area ratio. In [13], the optimization was carried out mostly based on the finite element (FE) method and results were qualitatively analyzed. The aforementioned two ratios were analytically derived for a fixed torque so the copper loss is not fixed. Moreover, the derivation excludes EWs, which can affect the optimal design parameters [23]. The multi-objective design optimization of WFSF machines for geared wind turbines was carried out in [24], but insightful guidance on design parameters cannot be provided due to the black box property of the algorithms. Although a simplified analytical model has been proposed for conventional WF machines with armature and DC windings located separately in the stator and rotor [25], the optimal parameters may differ in WFSF machines.

Therefore, as an extension of the work in [26], the optimal design for the maximum torque of the typical WFSF machines (Fig. 1) is investigated with a fixed copper loss. The WFSF machines with and without considering EWs are compared by the FE method, with particular attention paid on the influence of EWs. The results are then explained through a simplified analytical model accounting for the saturation, which cannot be neglected in WF machines. Key design parameters including the DC to armature winding copper loss ratio, slot area ratio and split ratio are taken into account. The influence of other design parameters is also investigated on the optimal split ratio. Finally, the electromagnetic performance of three optimized WFSF machines are compared.

II. Simplified Model Accouting For EWs

As noted, different DC winding configurations lead to different EW lengths. Hence, the simplified EW models of two machines are firstly built in order to investigate its influence. Moreover, the torque equation is deduced for later analysis.

The diagram of the WFSF machine is shown in Fig. 2. The adjacent slots contain DC and armature coils, respectively. With the same stator-/rotor- pole number combination, the allocation of armature windings in two machines are the same while the number of WF coils results in the difference.

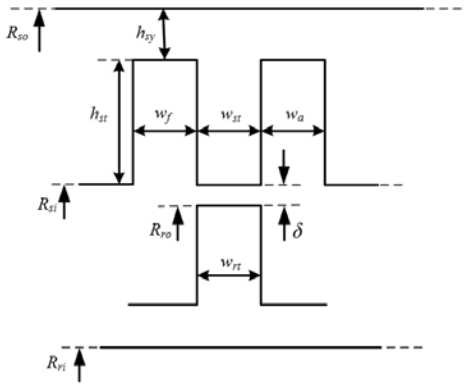

Fig. 2. Diagram of the WFSF machine.

In the model, the half turn of the EW is assumed to be an arc, as depicted in Fig. 3. The two coils of the armature windings in one slot share the slot area equally, as Fig. 3(a) shows. The active length of the armature coil is placed in a quarter of the width of the slot. As for the field coil, in Machine A, it is the same as the armature coil while in Machine B, the active part of the DC coil is considered to be in the middle of the slot, as plotted in Fig. 3(b).

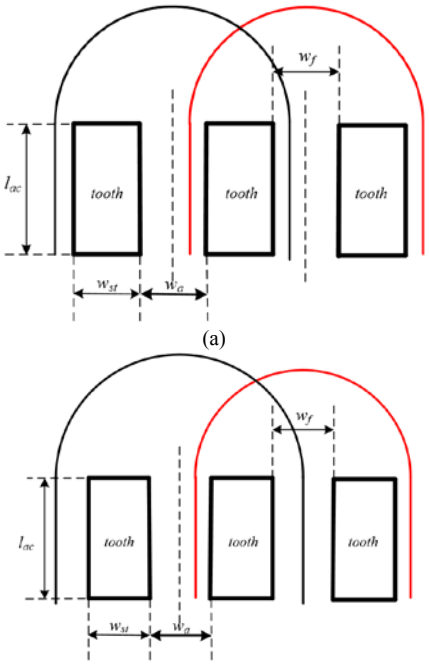

Fig. 3. Simplified model of coils including the EW in two machines. (a) Machine A. (b) Machine B.

The radii of EWs of armature and field coils in Machine A are assumed to be

$$\begin{cases} d_{aA} = \dfrac{\pi D_{so}\lambda}{N_s}[1-\dfrac{1}{2}(1-\gamma)k_{sa}] \\ d_{fA} = \dfrac{\pi D_{so}\lambda}{N_s}[1-\dfrac{1}{2}(1-\gamma)(1-k_{sa})] \end{cases} \tag{1}$$

where λ is the split ratio, γ is the flux density ratio, and k_{sa} is $S_a/(S_a+S_f)$. In Machine B, they are

$$\begin{cases} d_{aB} = d_{aA} \\ d_{fB} = \dfrac{\pi D_{so}\lambda}{N_s} \end{cases} \tag{2}$$

The active length of each coil is

$$l_{aacA} = l_{facA} = l_{aacB} = l_{facB} = 2l_{ac} \tag{3}$$

Therefore, for Machine A, the length of each armature coil can be expressed by:

$$l_{aA} = 2l_{ac} + \pi d_{aA} \tag{4}$$

When the machine operates with zero d-axis armature current control, and neglecting the iron loss, the normalized average electromagnetic (EM) torque is given by [25]:

$$TD = T / k_T = \lambda B_\delta N_{ac} I_a \tag{5}$$

where k_T is a coefficient related to the machine size and B_δ is the air-gap flux density. The relation between the armature copper loss and $N_{ac}I_a$ is given by:

$$P_{cua} = 24 I_a^2 \frac{\rho l_{aA} N_{ac}^2}{S_a k_{pa}} \tag{6}$$

The DC copper loss is expressed by:

$$P_{cuf} = 24 I_f^2 \frac{\rho l_f N_{fc}^2}{S_f k_{pf}} \tag{7}$$

where I_a and I_f are the armature and DC currents, respectively, and ρ is the electrical resistivity of copper. Each DC coil in Machine B has twice as many turns as the one in Machine A. Hence, only the DC coil length distinguishes between two machines, but the expressions of DC copper loss are identical when all other parameters are the same.

Based on the magnetic and geometric relationships, the slot area can be determined as follows:

$$S_a = \frac{\pi D_{so}^2 k_{sa}}{4N_s}\left(1-\frac{\pi}{N_s}\lambda\gamma-2\lambda\gamma+\lambda\right)\left(1-\frac{\pi}{N_s}\lambda\gamma-\lambda\right) \tag{8}$$

$$S_f = \frac{\pi D_{so}^2 (1-k_{sa})}{4N_s}\left(1-\frac{\pi}{N_s}\lambda\gamma-2\lambda\gamma+\lambda\right)\left(1-\frac{\pi}{N_s}\lambda\gamma-\lambda\right) \tag{9}$$

In WF machines, the saturation effect can be severe, especially when extremely high electric loading is applied. In such a circumstance, the reluctance of iron cores cannot be neglected. Therefore, an equivalent air-gap length is introduced to roughly reflect the saturation effect and calculate B_δ. By assuming the average relative permeability of stator and rotor cores being μ, the equivalent air-gap accounting for the reluctance of iron can be written as

$$\delta' = \delta + \frac{(1-\lambda k_{ri})D_{so}}{2\mu} \tag{10}$$

$$k_{ri} = \frac{D_{ri}}{\lambda D_{so}} \tag{11}$$

Based on (10), the air-gap flux density can be deduced by:

$$B_\delta = \mu_0 N_f I_f / \delta' = \frac{\mu_0}{\delta'}\sqrt{\frac{P_{cuf} S_f k_{pf}}{24\rho l_f}} \tag{12}$$

Then, the normalized torque can be further written as

$$TD = \frac{\mu_0 \pi D_{so}^2 \sqrt{k_{pf} k_{pa}} P_{cuf} P_{cua} k_{sa}(1-k_{sa})}{96\rho N_s} f(\lambda,\gamma) \tag{13}$$

$$f(\lambda,\gamma) = \frac{\lambda(1-\frac{\pi}{N_s}\lambda\gamma-2\lambda\gamma+\lambda)(1-\frac{\pi}{N_s}\lambda\gamma-\lambda)}{\delta'(\lambda)\sqrt{l_f(\lambda,\gamma) l_a(\lambda,\gamma)}} \tag{14}$$

III. Optimal Designs of WFSF Machines With and Without EWs

In this section, three key parameters are discussed to achieve the maximum torque under a fixed copper loss and overall size. The iron loss, however, which is usually dominant in high-speed machines [27], is neglected in this paper due to a low frequency of the investigated machine. TABLE I lists initial design parameters of the WFSF machine. The selected stator-/rotor-pole number is 12/10 to obtain a high torque density and eliminate the unbalanced magnetic force [28]. To emphasize the effect of EWs, a small aspect ratio (l_{ac}/D_{so}) is selected. It should be noted that a WFSF machine without considering EWs is also optimized for the comparison, whose coil length is $2l_{ac}$.

TABLE I
Design Parameters of WFSF Machine

Parameter	Symbol	Value
Number of stator poles	N_s	12
Number of rotor teeth	N_r	10
Number of stator phases	m	3
Active axial length	l_{ac}	25 mm
Stator outer diameter	D_{so}	90 mm
Split ratio	λ	0.6
Flux density ratio	γ	0.5
Stator back-iron thickness to stator tooth arc ratio	h_{sy_st}	1
Air-gap length	δ	0.5 mm
Rotor tooth arc to rotor tooth pitch ratio	k_{rt}	0.3
Number of turns per armature coil	N_{ac}	18
Number of turns per DC coil (double-layer)	N_{fcA}	12
Number of turns per DC coil (single-layer)	N_{fcB}	24
Slot package factor	k_{pf}, k_{pa}	0.4
DC to armature winding slot area ratio	S_f/S_a	1
DC to armature winding copper loss ratio	P_{cuf}/P_{cua}	1
Total copper loss	P_{cu}	37 W
Rated speed	n	400 rpm

A. DC to Armature Winding Copper Loss Ratio

When the total copper loss is fixed, we can have:

$$P_{cu} = P_{cua} + P_{cuf} \tag{15}$$

Substituting (15) into (13) and eliminating P_{cuf}, the maximum torque can be obtained by:

$$\partial TD / \partial P_{cua} = 0 \tag{16}$$

which leads to:

$$P_{cuf} = P_{cua} \tag{17}$$

Therefore, DC and armature windings should evenly share the copper loss to realize the greatest torque. It can be explained that when the fields excited by the DC and armature currents contribute equally, the maximum torque occurs. Moreover, this conclusion is independent of EWs.

Fig. 4(a) shows the FE-predicted electromagnetic torque of

three WFSF machines. Under the same copper loss, the average torques of Machines A and B are nearly half of that in the machine without EWs. It is because the aspect ratio is quite small, resulting in nearly equal active length and EW length. As a result, only a half of the copper loss is effective to generate the torque. In terms of the optimal DC to armature winding copper loss ratio, FE results show three WFSF machines all achieve their maximum torques when this ratio is unity, validating the analytical optimal value.

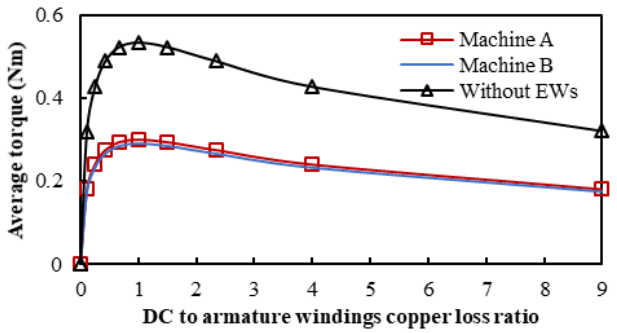

Fig. 4. Torque variations with the DC to armature winding copper loss ratio.

B. DC to Armature Windings Slot Area Ratio

The optimal slot area ratio for the maximum torque can be deduced likewise. With $P_{cuf} = P_{cua}$, TD is related only to the slot area and coil length. Substituting (1) into (13), for Machine A,

$$TD \propto \sqrt{\frac{k_{sa}(1-k_{sa})}{a^2 - ab + b^2 k_{sa}(1-k_{sa})}} \tag{18}$$

$$a = 2l_{ac} + \frac{\pi^2 D_{so}\lambda}{N_s}, b = \frac{\pi^2 D_{so}\lambda}{2N_s}(1-\gamma) \tag{19}$$

For a given split ratio and flux density ratio, by differentiating TD by k_{sa}, the maximum TD can be achieved when

$$(1-2k_{sa})a(a-b) = 0 \tag{20}$$

Since $a>b$ based on (19), (20) is satisfied only when k_{sa}=1/2. It means the DC slot area should be equal to the armature slot area for Machine A. Moreover, it is also the optimal solution for the machine without EWs ($d_a = d_f = 0$). Nevertheless, for Machine B, (20) becomes:

$$bk_{sa}^2 + a(1-2k_{sa}) = 0 \tag{21}$$

(21) indicates that (1-2k_{sa}) must be negative to achieve the maximum torque in Machine B. In other words, the armature slot area must be larger than the DC slot area. To be specific, the optimal k_{sa} is

$$k_{sap} = \frac{a - \sqrt{a(a-b)}}{b} \tag{22}$$

According to the analytical derivation, when the slot area ratio is unity, the maximum torque is obtained in WFSF machines with double-layer DC and armature windings. For the WFSF machine with single-layer DC windings, the DC slot is preferred to be smaller than the armature slot. It has been pointed out that when the contributions of two fields are equal, the maximum torque can be attained. Due to longer EWs, the DC coil length in Machine B is longer than the armature coil length when two slots areas are the same. This results in a larger R_f and hence a lower $N_f I_f$. Hence, the DC slot width should be reduced to compensate for the difference between the two windings in Machine B. Additionally, the optimal slot area ratio depends on a and b in (19). For example, the variation of the active length can greatly change a while b remains constant. Fig. 5 depicts the analytically optimal slot area ratio for Machine B obtained based on (22) when the active length varies. It can be seen when the aspect ratio increases, the difference in winding lengths is narrowed down. As a result, the optimal slot area ratio increases with the aspect ratio and approaches to unity infinitely.

Fig. 6 shows the analytical and FE-predicted torques against the slot area ratio. The torque when S_f=S_a is refereed as the unit torque in two models, respectively. As illustrated in Fig. 7, the stator tooth width remains constant in the FE model while the slot opening varies with the corresponding slot area ratio. Analytically, Machine A and the machine without EWs have the same trends, and both of their optimal slot area ratios are unity. As for Machine B, the analytical optimal slot area ratio is 0.94 under the machine size in TABLE I. However, it turns out that the optimal slot area ratios obtained by the FE method are 1.22, 1.22 and 1.13 for the machine without EWs, Machines A and B, respectively, which are all larger than the analytical optimal ratios. It is mainly because of magnetic saturation and flux leakage. When linear materials are adopted in the iron core, the FE-predicted optimal ratios would come closer to unity, which is 1.1 for Machine A, but they would still be larger due to the inevitable flux leakage. In the linear model, some of fluxes generated by the DC field would still leak though slots, which lower the phase flux linkage. Thus, by enlarging the DC slot area properly, the DC field can be effectively enhanced due to a larger current when the copper loss is fixed. It is noteworthy that the average torque is already up to 98% to 99% of the maximum torque when the slot area ratio is unity in the FE model. Consequently, the equal slot areas can be taken as a rule of thumb.

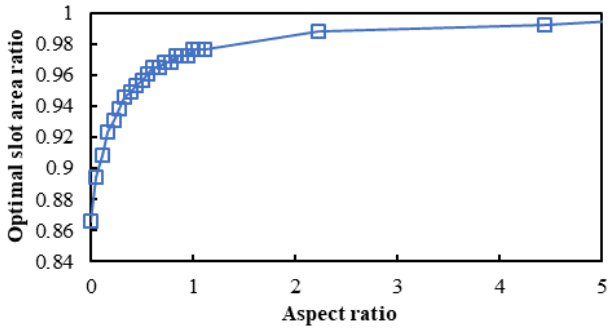

Fig. 5. Optimal slot area ratio for Machine B when the aspect ratio varies.

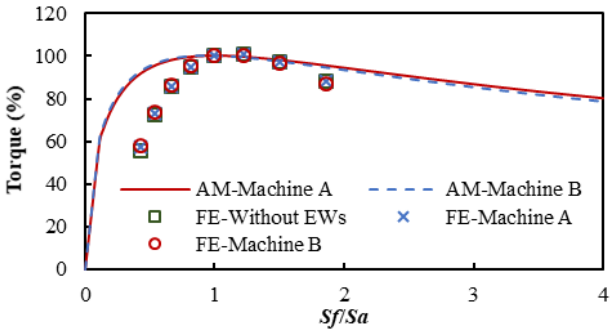

Fig. 6. Variation of the average torque with the DC to armature slot area ratio.

Fig. 7. WFSF machines with different DC to armature slot area ratios. (a) S_f/S_a=1.5. (b) S_f/S_a=1.

C. Split Ratio

The torque capability is sensitive to the split ratio due to its effect on slot areas and hence the currents. Applying the optimal slot area ratio and copper loss ratio, TD in (13) for the machine without EWs can be written by:

$$TD \propto \lambda(1-\frac{\pi}{N_s}\lambda\gamma-2\lambda\gamma+\lambda)(1-\frac{\pi}{N_s}\lambda\gamma-\lambda)/\delta^{'}=TD^{'} \quad (23)$$

For Machine A, it can be expressed by:

$$TD \propto \frac{TD'}{\sqrt{a^2-ab+b^2/4}} \quad (24)$$

and

$$TD \propto \frac{TD'}{\delta^{'}\sqrt{a(a-b/2)}} \quad (25)$$

for Machine B. According to (10), the saturation effect has a greater influence on the equivalent air-gap, which depends largely on the flux density ratio. Hence, for a given flux density ratio, the equivalent air-gap length can be assumed to be a constant. Then, the optimal split ratio can be deduced. For the machine without EWs, it is

$$\lambda_{op}=\frac{c+d\pm\sqrt{c^2+d^2-cd}}{3cd} \quad (26)$$

$$c=\frac{\pi}{N_s}\gamma+2\gamma-1, d=\frac{\pi}{N_s}\gamma+1 \quad (27)$$

Based on (19), $a(a\text{-}b)+b^2/4$ and $a(a\text{-}b/2)$ both increase with the split ratio. Therefore, it can be expected that the optimal split ratios of Machines A and B will be smaller than that of the machine without EWs.

Fig. 8 depicts torque variations with the split ratio by the FE method. The average torque firstly rises with the split ratio and then decreases. Fig. 9 shows the current declines with the split ratio while the phase back-EMF shows a similar trend to the torque variation. Theoretically, the variation of the phase back-EMF would be consistent with the DC current trend. However, differences occur when the split ratio is small due to severer flux leakage. Consequently, the maximum torque exists.

It can be found in Fig. 8 that the optimal split ratios in Machines A and B are smaller, which is consistent with what the analytical model predicts. The optimal split ratios are around 0.5 for Machines A and B and it is around 0.6 if EWs are not considered. Based on FE results, if Machines A and B are applied with the optimal split ratio of the machine without EWs, the torque loss is around 12%. It can be explained from the perspective of the magnetic field in addition to the analytical model. When the flux density ratio is fixed, the variation of the split ratio leads to different tooth widths and hence different slot areas. If EWs are not considered, only slot areas rather than coil lengths are related to the split ratio. Nevertheless, with the optimal split ratio in the machine without EWs, the slot and tooth widths lead to longer EWs and hence less effective copper loss and weaker magnetic fields in Machines A and B. As a result, larger space and shorter EWs for coils are preferred and the optimal split ratio is smaller if EWs are considered. Although EW lengths of DC coils differ, Machines A and B have basically the same optimal split ratios.

IV. Influence of Design Parameters on Optimal Split Ratio of WFSF Machine

For the optimal split ratio, (26) demonstrates that it is related to other parameters as well. Hence, in this section, the influence of design parameters on the optimal split ratio is addressed taking Machine A as an example.

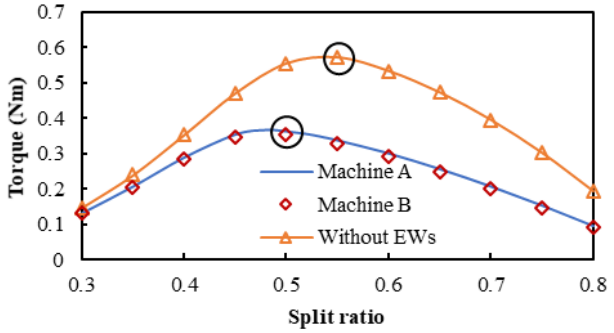

Fig. 8. FE-predicted torque variation with the split ratio, γ=0.5.

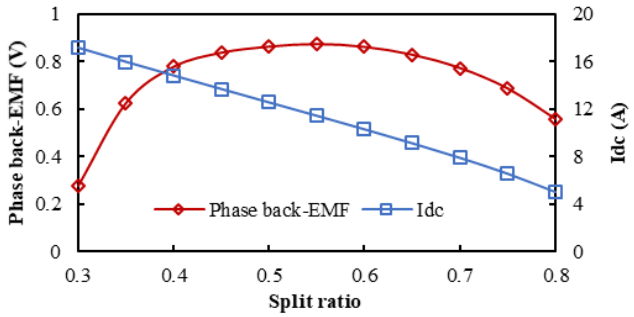

Fig. 9. Phase back-EMF and I_f variations with the split ratio.

A. Flux Density Ratio

Fig. 10 shows the torque characteristics with different split ratios and flux density ratios and there always exists an optimal split ratio. With a given copper loss and split ratio, a smaller flux density ratio leads to a larger magnetomotive force due to larger slot areas and hence the heavier electric loading. Consequently, the flux density in stator iron also increases, which aggravates the saturation and lengthens the equivalent air-gap according to (10). It can be seen in Fig. 10, when the split ratio is around 0.3 to 0.4, the torque increases firstly with the flux density ratio and then levels off since stator teeth are wider and the equivalent air-gap length is almost a constant value. At this stage, the variation of the equivalent air-gap is dominant in the determination of the torque. When the split ratio keeps increasing, the torque increases at first for the same reason but then diminishes. It is because the equivalent air-gap length is a constant value and then the variation of slot areas has a greater effect on the torque. With a larger flux density ratio and hence a wider tooth width, slots get smaller and the magnetomotive force gets weaker, resulting in a decreased

torque. As for the optimal split ratio, it decreases with the flux density ratio due to the co-effect of the saturation and slot area variation, as Fig. 11 presents. Overall, when the tooth width equals the slot opening width, the torque is optimal for any given split ratio.

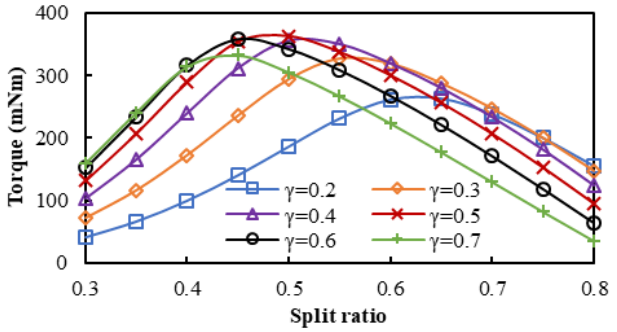

Fig. 10. FE-predicted average torque with λ and γ.

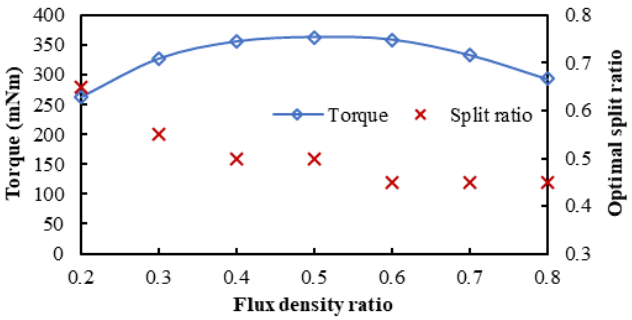

Fig. 11. Optimal split ratio and corresponding maximum torque variations with the flux density ratio.

B. *Copper Loss*

As been noted, the magnetomotive force is directly determined by the copper loss and further influences the torque. Considering that WF machines should be capable of withstanding high electric loading, different copper losses are applied to the machine to investigate its influence on the optimal split ratio. As Fig. 12 shows, the optimal split ratio slightly increases with the copper loss but mostly focuses on the range of 0.5 to 0.55. For a certain flux density ratio, higher currents cause the flux density in iron to increase, which has been cited that the equivalent air-gap will then be longer. Consequently, the split ratio should properly increase so the tooth width is wider and the current is reduced, eventually reaching the most balanced state to achieve the maximum torque.

C. *Air-gap Length*

The air-gap length is critical for the torque no matter in PM machines or WF machines. Fig. 14 shows the torque decreases with the air-gap for a given split ratio due to the larger reluctance in the air-gap. Moreover, it can be seen the torque of the WFSF machine is quite sensitive to the air-gap length. In Fig. 15, the analytical optimal split ratio is basically the same even though the air-gap changes. From (10), the equivalent air-gap increases with the actual air-gap length, resulting in reduced torque. Generally, even though the equivalent air-gap length is related to the split ratio, the effect on the optimal split ratio is rather small. The slight increase can be explained by the flux leakage. In practice, when the split ratio and the flux density ratio are the same, the increasing air-gap length results in more fluxes leaking through stator teeth rather than being modulated by the rotor teeth. With a large split ratio, the magnetic leakage can be eased because of wider slot openings. It should be noted that the leakage variation is mild so the optimal split ratio only rises slightly with the air-gap length.

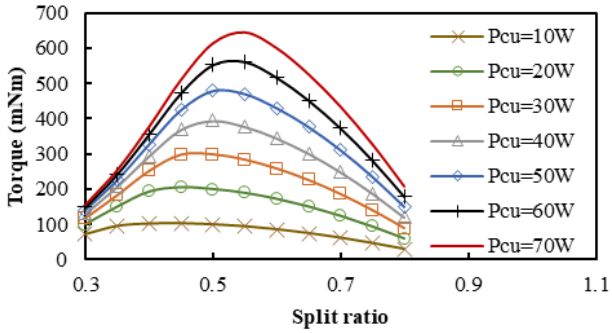

Fig. 12. Torque variations with the split ratio and total copper loss.

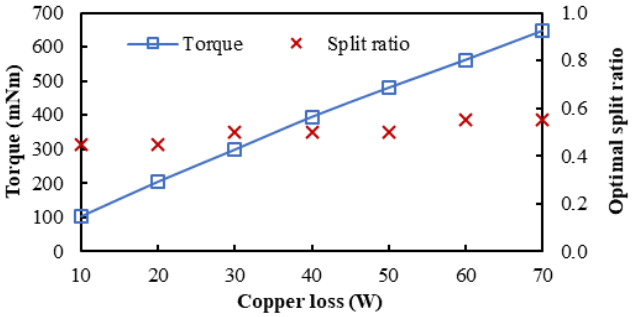

Fig. 13. Optimal split ratio and the corresponding maximum torque variations with the total copper loss.

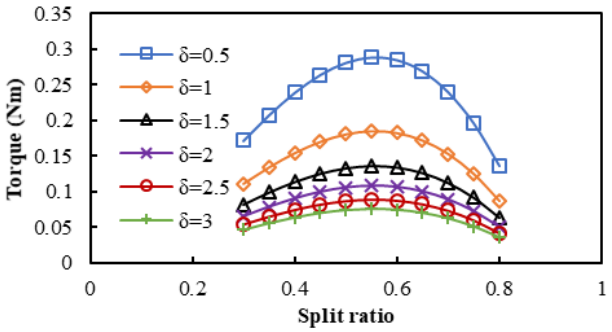

Fig. 14. FE-predicted average torque with the air-gap length.

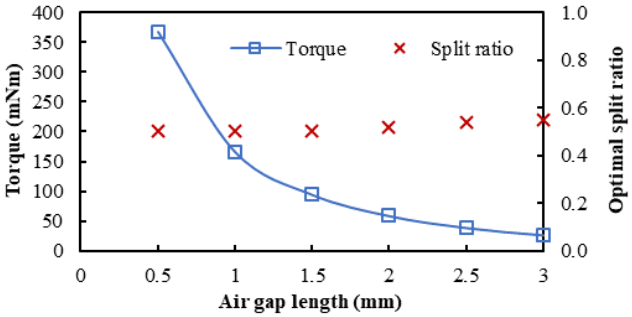

Fig. 15. Optimal split ratio and corresponding maximum torque when the air-gap varies.

D. *Aspect Ratio*

It has been studied that a smaller aspect ratio helps to achieve

larger torque output when the overall volume is fixed. In Fig. 15, it validates this conclusion even though the EWs occupy a big portion of the copper loss when the aspect ratio is small. As for the optimal split ratio, it slightly decreases with the aspect ratio.

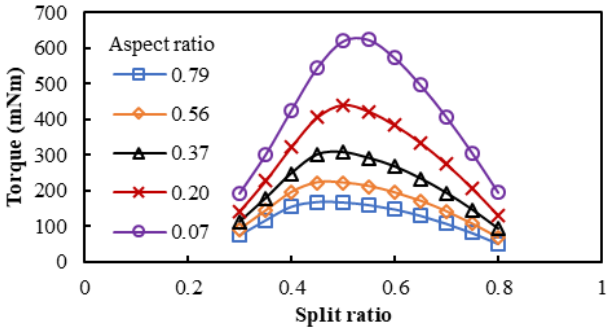

Fig. 16. Variation of average torque with split ratio and total copper loss.

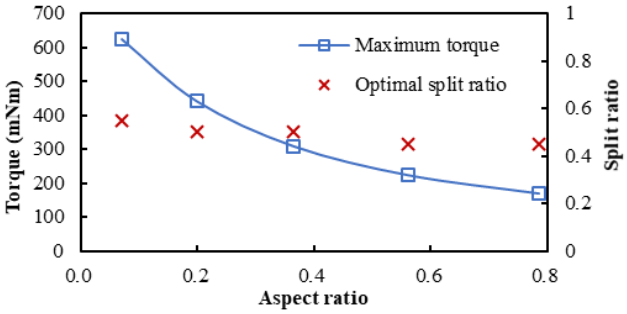

Fig. 17. Variation of the optimal split ratio and corresponding maximum torque with the aspect ratio.

V. Compasiron of Electromagnetic Performance

The initial and optimal designs with and without EWs are shown in Fig. 17, and their optimal key parameters are listed in TABLE II. As can be seen, the optimal split ratios are smaller in machines with EWs. In addition, Machine B has a smaller optimal split ratio than Machine A, but the difference is minor. As for the flux density ratio, the maximum torque can be achieved when the tooth and slot widths are equal. Fig. 19 and Fig. 20 show the phase back-EMFs and torque waveforms of three optimized WFSF machines. The machine without EWs has the largest phase back-EMF due to stronger DC and armature fields under the same copper loss. Between Machines A and B, they exhibit similar back-EMF waveforms because of similar optimal designs. To be more specific, the higher back-EMF and larger currents in Machine A lead to about 6.6% larger torque than that in Machine B with longer EWs, as compared in TABLE III. Compared with the machine without consideration of EWs, WFSF machines with EWs can achieve a 60% torque under the same copper loss due to lower back-EMFs and much lower currents. Through optimization, three machines experience 26%, 34% and 32% increase in torque, respectively.

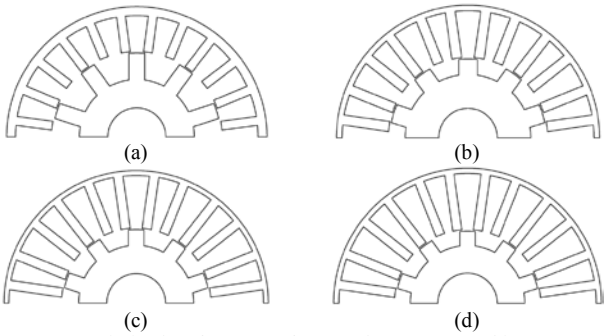

Fig. 18. Optimized 12/10 stator-/rotor-pole WFSF machines. (a) Original machine. (b) Machine without EWs. (c) Machine A. (d) Machine B.

TABLE II
Optimal Design of the WFSF Machines

Parameters	Without EWs	Machine A	Machine B
S_f/S_a	1.291	1.283	1.203
k_{fa}	1	1	1
Split ratio	0.6	0.56	0.54
Flux density ratio	0.5	0.5	0.5

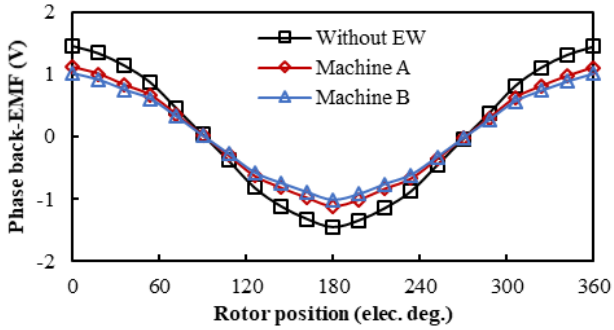

Fig. 19. Comparison of back-EMF of optimized WFSF machines.

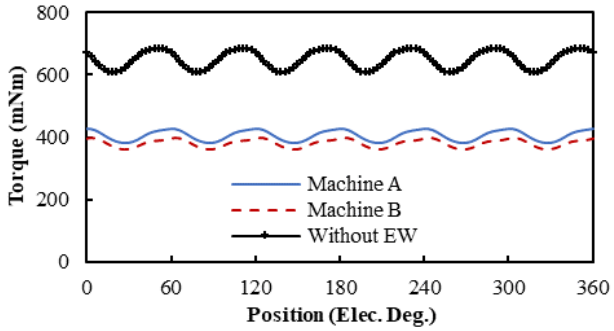

Fig. 20. Torque waveforms of three WFSF machines.

TABLE III
Torque Comparison of Original and Optimal WFSF Machines

	Without EWs	Machine A	Machine B
Original	0.515 Nm	0.303 Nm	0.288 Nm
Optimized	0.650 Nm	0.406 Nm	0.381 Nm

VI. Conclusion

In this paper, optimal design parameters for the maximum torque of 12/10 stator-/rotor-pole WFSF machines are investigated under the fixed copper loss. The WFSF machines include one machine without EWs, Machine A with double-layer DC windings and Machine B with single-layer DC windings. It is discovered the maximum torque can be realized when the copper loss is equally shared by DC and armature windings for all the machines. If the machine with both double-layer DC and armature windings, the slot area ratio is preferred to be unity. For Machines B, however, smaller DC slots than the armature slot area are desired and the slot area

ratio approaches to unity as the aspect ratio increases. In addition, the optimal split ratio decreases with longer EWs since such machines require larger slot areas to achieve higher currents.

Furthermore, the flux density ratio also has a significant influence on the optimal split ratio. On the one hand, the flux density ratio determines the slot areas and hence the currents. On the other hand, according to the analytical model, the severe saturation in WF machines leads to considerable magnetic reluctance in the iron and hence the increased equivalent air-gap length when the flux density ratio is small. Consequently, the optimal split ratio is larger in this case so the currents are reduced to cooperate with wider tooth widths, and then the iron can be fully utilized to achieve the maximum torque.

Overall, with a fixed copper loss, the WFSF machine with both double-layer DC and armature windings has superior performance than that with single-layer DC windings.

REFERENCES

[1] M. Cheng, W. Hua, J. Zhang, and W. Zhao, "Overview of stator-permanent magnet brushless machines," *IEEE Trans. Ind. Electron.*, vol. 58, no. 11, pp. 5087–5101, Nov. 2011.

[2] J. T. Chen and Z. Q. Zhu, "Winding configurations and optimal stator and rotor pole combination of flux-switching PM brushless AC machines," *IEEE Trans. Energy Convers.*, vol. 25, no. 2, pp. 293–302, Jun. 2010.

[3] Z. Q. Zhu, Y. Pang, J. T. Chen, Z. P. Xia, and D. Howe, "Influence of design parameters on output torque of flux-switching permanent magnet machines," in *Proc. IEEE Veh. Power Propuls. Syst. Conf.*, Sep. 2008, pp. 1–6.

[4] L. Wu, J. Zhu and Y. Fang, "A novel doubly-fed flux-switching permanent magnet machine with armature windings wound on both stator poles and rotor teeth," *IEEE Trans. Ind. Electron.*, vol. 67, no. 12, pp. 10223-10232, Dec. 2020.

[5] Z. Q. Zhu, Y. Pang, D. Howe, S. Iwasaki, R. Deodhar, and A. Pride, "Analysis of electromagnetic performance of flux-switching permanent magnet machines by non-linear adaptive lumped parameter magnetic circuit model," *IEEE Trans. Magn.*, vol.41, no.11, pp.4277-4287, 2005.

[6] I. Boldea, Z. Jichun, and S. A. Nasar, "Theoretical characterization of flux reversal machine in low-speed servo drives-the pole-PM configuration," *IEEE Trans. Ind. Appl.*, vol. 38, no. 6, pp. 1549–1557, Nov./Dec. 2002.

[7] C. X. Wang, I. Boldea, and S. A. Nasar, "Characterization of three phase flux reversal machine as an automotive generator," *IEEE Trans. Energy Convers.*, vol. 16, no. 1, pp. 74–80, Mar. 2001.

[8] L. Wu, G. Ming, L. Zhang, Y. Fang, T. Li, and W. Zheng, "Comparative Study Between Doubly Salient PM Machine With New Stator/Rotor-Pole Number Combination and Biased Flux PM Machine," *IEEE Trans. Ind. Appl.*, vol. 57, no. 3, pp. 2354–2365, May 2021.

[9] R. Cao, X. Yuan, Y. Jin, and Z. Zhang, "MW-Class Stator Wound Field Flux-Switching Motor for Semidirect Drive Wind Power Generation System," *IEEE Trans. Ind. Electron.*, vol. 66, no. 1, pp. 795–805, Jan. 2019.

[10] A. Fasolo, L. Alberti, and N. Bianchi, "Performance comparison between switching-flux and IPM machines with rare-earth and ferrite PMs," *IEEE Trans. Ind. Appl.*, vol. 50, no. 6, pp. 3708–3716, Nov. 2014.

[11] H. Wei, Z. Gan, and C. Ming, "Flux-regulation theories and principles of hybrid-excited flux-switching machines," *IEEE Trans. Ind. Electron.*, vol. 62, no. 9, pp. 5359–5369, Sep. 2015.

[12] E. Hoang, M. Lecrivain, and M. Gabsi, "A new structure of a switching flux synchronous polyphased machine with hybrid excitation," in *Proc. Eur. Conf. Power Electron. Appl.*, Sep. 2007, pp. 1–8.

[13] J. T. Chen, Z. Q. Zhu, S. Iwasaki and R. Deodhar, "Low cost flux-switching brushless AC machines," in *Proc. IEEE Veh. Power Propuls. Conf.*, Sept. 2010, pp. 1-6.

[14] C. Pollock and M. Wallace, "The flux-switching motor, a DC motor without magnets or brushes," in *Proc. IEEE Ind. Appl. Soc. Annu. Meeting*, Oct. 1999, pp. 1980–1987.

[15] Z. Z. Wu, Z. Q. Zhu, C. Wang, J.-C. Mipo, S. Personnaz, and P. Farah, "Analysis and reduction of on-load DC winding induced voltage in wound field switched flux machines," *IEEE Trans. Ind. Electron.*, vol. 67, no. 4, pp. 2655–2666, Apr. 2020.

[16] A. Zulu, B. C. Mecrow, and M. Armstrong, "A Wound-Field Three-Phase Flux-Switching Synchronous Motor With All Excitation Sources on the Stator," *IEEE Trans. Ind. Appl.*, vol. 46, no. 6, pp. 2363–2371, Nov. 2010.

[17] M. F. Omar, E. Sulaiman, M. Jenal, R. Kumar, and R. N. Firdaus, "Magnetic flux analysis of a new field-excitation flux switching motor using segmental rotor," *IEEE Trans. Magn.*, vol. 53, no. 11, pp. 1–4, Nov. 2017.

[18] Z. Q. Zhu, Z. Z. Wu, D. J. Evans, and W. Q. Chu, "A wound field switched flux machine with field and armature windings separately wound in double stators," *IEEE Trans. Energy Convers.*, vol. 30, no. 2, pp. 772–783, Jun. 2015.

[19] S. Jia, R. Qu, J. Li, D. Li, and H. Lu, "Comparison of stator DC current excited Vernier reluctance machines with different field winding configurations," *IEEE Trans. Magn.*, vol. 53, no. 6, Jun. 2017, Art. no. 8103504.

[20] W. Jiang, W. Huang, X. Lin, Y. Zhao, and S. Zhu, "Analysis of rotor poles and armature winding configurations combinations of wound field flux switching machines," *IEEE Trans. Ind. Electron.*, vol. 68, no. 9, pp. 7838–7849, Sep. 2021.

[21] J. T. Chen and Z. Q. Zhu, "Influence of rotor pole number on optimal parameters in flux-switching PM brushless AC machines by lumped parameter magnetic circuit model," in *Proc. IEEE Int. Elect. Mach. Drives Conf.*, Miami, FL, USA, May 2009, pp. 1216–1223.

[22] J. T. Shi, X. Liu, D. Wu, and Z. Q. Zhu, "Influence of Stator and Rotor Pole Arcs on Electromagnetic Torque of Variable Flux Reluctance Machines," *IEEE Trans. Magn.*, vol. 50, no. 11, pp. 1–4, Nov. 2014.

[23] Y. Shen, Z. Q. Zhu, and L. J. Wu, "Analytical determination of optimal split ratio for overlapping and none-overlapping winding external rotor PM brushless machines," in *Proc. IEEE Int. Elect. Mach. Drive Conf.*, May 2011, pp. 41-46.

[24] U. B. Akuru and M. J. Kamper, "Formulation and multiobjective design optimization of wound-field flux switching machines for wind energy drives," *IEEE Trans. Ind. Electron.*, vol. 65, no. 2, pp. 1828–1836, Feb. 2018

[25] W. Q. Chu, Z. Q. Zhu, and J. T. Chen, "Simplified analytical optimization and comparison of torque densities between electrically excited and permanent magnet machines," *IEEE Trans. Ind. Electron.*, vol. 61, no. 9, pp. 5000–5011, Sep. 2014.

[26] W. Wang, L. Wu and J. Zhu, "Influence of End-Winding on Optimal Design Parameters for Maximum Torque of DC Excited Flux-Switching Machines, " in *Proc. IEEE Int. Conf. Elect. Mach. Sys.*, 2019, pp. 1-6.

[27] Y. Wang, S. Guo, Y. Li, Z. Chen, Y. Wang, and Z. Zhu, "Investigation of optimal split ratio for high-speed permanent magnet brushless machines," *IEEE Trans. Magn.*, vol.54, no.11, 2018.

[28] J. Zhu and L. Wu, "Winding Configurations and Pole/Tooth Combinations of Doubly-Fed Flux-Switching Permanent Magnet Machines," *IEEE Trans. Ind. Electron.*, vol. 69, no. 3, pp. 2380-2389, March 2022.

Wenting Wang received the B.Eng. degree in electrical engineering in 2019 from Zhejiang University, Hangzhou, China, where she is currently working toward the Ph.D. degree in electrical engineering.

Her major research interest is the design of permanent magnet machines.

Yuankui Wang received the M.Sc. degrees in electrical engineering from Jiangsu University, Zhenjiang, China, in 2004. And now, he is pursuing the Ph.D. degree in Zhejiang University, Hangzhou, China.

Since 2004, he has been with the Kunming Branch of the 705 Research Institute, China State Shipbuilding Corporation, Ltd., Kunming, China, where he is currently a professor-level senior engineer. His current research focuses on permanent magnet machines and controller.

Enlin Ma received the B.Eng. degree in electrical engineering from Harbin institute of technology, Harbin, China, in 2004. Since 2004, he has been with Xi'an Research Institute of precision mechanics, China State Shipbuilding Corporation, Ltd.. His current research focuses on design of special electrical machines.

Lijian Wu (M'11-SM'14) received the B.Eng. and M.Sc. degrees from Hefei University of Technology, Hefei, China, in 2001 and 2004, respectively, and the Ph.D. degree from the University of Sheffield, Sheffield, U.K., in 2011, all in electrical engineering.

From 2004 to 2007, he was an Engineer with Delta Electronics (Shanghai) Co, Ltd. From 2012 to 2013, he was with Sheffield Siemens Wind Power Research Center as a design engineer focusing on wind power generators. From 2013 to 2016, he was an advanced engineer with Siemens Wind Power A/S in Denmark. Since 2016, he has been with Zhejiang University, where he is currently Professor of electrical machines and control systems. His major research interests include design and control of permanent magnet machines.